ISSN 0018-151X, High Temperature, 2017, Vol. 55, No. 6, pp. 887–897. © Pleiades Publishing, Ltd., 2017.
Original Russian Text © O.N. Goncharova, E.V. Rezanova, Yu.V. Lyulin, O.A. Kabov, 2017, published in Teplofizika Vysokikh Temperatur, 2017, Vol. 55, No. 6, pp. 720–732.

HEAT AND MASS TRANSFER AND PHYSICAL GASDYNAMICS

Analysis of a Convective Fluid Flow with a Concurrent Gas Flow with Allowance for Evaporation

O. N. Goncharova[a, b], E. V. Rezanova[a, b], Yu. V. Lyulin[b, c, *], and O. A. Kabov[b, c]

[a] *Altai State University, Barnaul, 656049 Russia*
[b] *Institute of Thermophysics, Siberian Branch, Russian Academy of Sciences, Novosibirsk, 630090 Russia*
[c] *National Research Tomsk Polytechnic University, Tomsk, 634050 Russia*
**e-mail: lyulin@itp.nsc.ru*

Received July 29, 2015

Abstract—The paper presents a theoretical analysis of a convective fluid flow with a concurrent gas flow accompanied by evaporation at the interface. The analysis of two-layer flows is based on a mathematical model taking into account evaporation at a thermocapillary boundary and effects of thermal diffusion and diffusion heat conduction in the gas–vapor layer. New exact solutions describing steady two-layer flows in a channel with the interface remaining undeformed and examples of velocity and temperature profiles for the HFE-7100 (liquid)–nitrogen (gas) system are presented. The influence of longitudinal temperature gradients along the channel boundaries, the gas flow rate, and the height of the fluid layer on the flow regime and evaporation rate is studied. A comparison of the calculated data with experimental results is performed.

DOI: 10.1134/S0018151X17060074

INTRODUCTION

Convective fluid flows accompanied by evaporation or condensation at the interface often arise under the action of concurrent gas flows and are being actively studied experimentally and theoretically [1–6]. After the creation of a new experimental setup [7], evaporative convection can be studied in still and moving layers under the action of dry and moist gas flows, which is the most important motivation for the development of the theory of convection in regions with interfaces, since it enables one to validate mathematical models and compare them with experimental data.

Mathematical models of convective motions with allowance for heat and mass transfer and with formulation of boundary conditions at the interface were developed in [3, 4, 8–11]. Of special interest are solutions of a specific type, describing two-layer or multilayer fluid flows in infinite channels with interfaces [12–17]. Constructing the exact solutions becomes especially important for the study of problems with allowance for heat and mass transfer at the interface, because they enable one to verify mathematical models, to study the influence of various physical factors on the flow regime and evaporation rate, and make prediction concerning the experiments, including those currently prepared at the International Space Station [3, 6, 18].

One of the first examples of exact solutions describing two-layer flows with allowance for the mass transfer was in [19] for the case of a liquid–liquid interface. In [14, 15], exact solutions were constructed for the problem of two-layer flow of a liquid and an isothermal gas in the complete formulation. The evaporation in [14, 15] is not taken into account explicitly but simulated by the condition for the temperature at the interface. Exact solutions describing two-layer flows with evaporation with allowance for the Dufour effect in the gas phase [20] were constructed in [21] for the case of a given gas flow rate and, in [18], under the conditions of closed flows in both phases. The solutions constructed in [13–15, 18, 19, 21] can be called a generalization of the well-known solution [22] for convection in an infinite layer with a nondeformable free boundary under the action of a transverse gravity field and a longitudinal temperature gradient.

The aim of this paper is an analytical study of steady fluid flows under the action of a concurrent gas flow with allowance for evaporation at the thermocapillary interface and, in addition, a comparison of the results with experimental data. The mathematical modeling of two-layer flows is performed with the help of exact solutions of the Navier–Stokes equations in the Oberbeck–Boussinesq approximation [23, 24]. In the upper layer, which is a gas–vapor mixture, the diffusion of vapor and effects of thermal diffusion and diffusive thermal conduction (the Soret and Dufour effects) are taken into account [20, 23, 25] (see also [26–29]). In these solutions, the longitudinal components of the fluid and gas velocity are nonzero and depend only on the transverse coordinate. The functions of temperature in the upper and lower layers, the vapor concentration in the gas, and the pressure

depend on both coordinates, linearly on the longitudinal coordinate.

In this work, we have exact solutions of the initial system of differential equations and propose not only a physical interpretation of these solutions but also compare the results of simulation of convective flows with evaporation based on these solutions with experimental data. Specific features of two-layered flows of a liquid (HFE-7100) and gas (nitrogen) and the evaporation rate of the liquid at the interface are studied. The influence of the variation in the gas flow rate, longitudinal temperature gradients, and the Soret effect on the velocity and temperature profiles and the mass of the liquid evaporating from the interface is shown. The comparisons of theoretical and experimental data reflecting the dependence of the evaporation rate from the free boundary on the gas flow rate and the thickness of the liquid layer are presented.

1. FORMULATION OF THE PROBLEM OF A TWO-LAYER FLOW WITH ALLOWANCE FOR EVAPORATION. CONSTRUCTING THE EXACT SOLUTION

Let two immiscible, viscous, and incompressible fluids (a liquid and a gas–vapor mixture) fill infinite layers of thickness l and h, respectively. The reference frame is chosen so that the gravitational vector $\mathbf{g}$ is directed against the axis Oy ($\mathbf{g} = (0,-g)$) (see Fig. 1). The upper and channel lower walls, $y = h$ and $y = -l$, comprise solid impermeable boundaries, and their interface $y = 0$ remains undeformed. The system of the Navier–Stokes equations in the Oberbeck–Boussinesq approximation is used to simulate the fluid flows in the lower and upper layers in the steady state. The concentration of vapor, which is considered a passive admixture, i.e., not affecting the properties of the gas, is described by the diffusion equation. Taking into account the Soret and Dufour effects in the gas layer, the mathematical model comprises the system of differential equations

$$u\frac{\partial u}{\partial x} + \upsilon\frac{\partial u}{\partial y} = -\frac{1}{\rho}\frac{\partial p'}{\partial x} + \nu\left(\frac{\partial^2 u}{\partial x^2} + \frac{\partial^2 u}{\partial y^2}\right), \qquad (1)$$

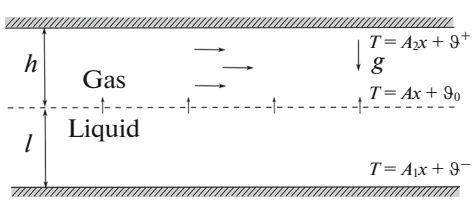

Fig. 1. Geometry of the flow region.

$$u\frac{\partial \upsilon}{\partial x} + \upsilon\frac{\partial \upsilon}{\partial y} = -\frac{1}{\rho}\frac{\partial p'}{\partial y} + \nu\left(\frac{\partial^2 \upsilon}{\partial x^2} + \frac{\partial^2 \upsilon}{\partial y^2}\right) + g(\beta T + \gamma C), \qquad (2)$$

$$\frac{\partial u}{\partial x} + \frac{\partial \upsilon}{\partial y} = 0, \qquad (3)$$

$$u\frac{\partial T}{\partial x} + \upsilon\frac{\partial T}{\partial y} = \chi\left(\frac{\partial^2 T}{\partial x^2} + \frac{\partial^2 T}{\partial y^2} + \delta\left(\frac{\partial^2 C}{\partial x^2} + \frac{\partial^2 C}{\partial y^2}\right)\right), \qquad (4)$$

$$u\frac{\partial C}{\partial x} + \upsilon\frac{\partial C}{\partial y} = D\left(\frac{\partial^2 C}{\partial x^2} + \frac{\partial^2 C}{\partial y^2} + \alpha\left(\frac{\partial^2 T}{\partial x^2} + \frac{\partial^2 T}{\partial y^2}\right)\right) \qquad (5)$$

with the boundary conditions formulated below. The terms γC and $\delta\Delta C$ in Eqs. (2) and (4) and Eq. (5) are used for the simulation of the flow in the upper layer. Here u and υ are the projections of the velocity vector on the axes of the Cartesian frame of reference, p' is the modified pressure or deviation from the hydrostatic pressure ($p' = p - \rho\mathbf{g}\cdot\mathbf{x}$, $\mathbf{x} = (x,y)$, p is pressure), T is temperature, C is the vapor concentration, ρ is the density (relative density), ν is the kinematic viscosity, χ is the thermal diffusivity, D is the diffusion coefficient of vapor in the gas, β is the thermal expansion coefficient, γ is the concentration density coefficient, δ is a coefficient characterizing the Dufour effect, and α is a coefficient characterizing the Soret effect in the gas–vapor layer.

Suppose that the solution $u_i, \upsilon_i, p_i', T_i$, and C of Eqs. (1)–(5) has the special form [19, 22]

$$u_i = u_i(y), \quad \upsilon_i = 0, \quad p_i' = p_i'(x,y),$$
$$T_i = (a_1^i + a_2^i y)x + \vartheta_i(y), \quad C = (b_1 + b_2 y)x + \varphi(y). \qquad (6)$$

If the functions or coefficients are marked with a lower or upper index i ($\underline{i} = 1, 2$), then, for $i = 1$, they characterize the fluid in the bottom layer and, for $i = 2$, the fluid (gas–vapor mixture) in the upper layer. Note that the system of equations (1)–(5), describing the convective motions of fluids, is rather complex not only because of its nonlinearity and high order but also because it does not belong to any classical type (see, e.g., [30]). Constructing the exact solutions in form (6) makes it possible to reduce the problem to solving equations of lower dimension and study flows caused by the combined effect of a longitudinal temperature gradient and transversely directed gravity force. A systematic analysis of the exact solutions of convection equations, including the determination of the type of solution, refers to problems solved using methods of group analysis of differential equations [31, 32]. The group nature of the Birikh solution [22] and possible generalizations of this solution to the three-dimensional case are discussed in [33], and the solutions of the Oberbeck–Boussinesq equations, in which the temperature function linearly depends on the longitudinal coordinate, were first in [34].

The solution of the system of equations (1)–(5) of form (6) can be represented as

$$u_i = \frac{y^4}{24}L_4^i + \frac{y^3}{6}L_3^i + \frac{y^2}{2}c_1^i + yc_2^i + c_3^i, \tag{7}$$

$$T_i = (a_1^i + a_2^i y)x + \frac{y^7}{1008}N_7^i + \frac{y^6}{720}N_6^i + \frac{y^5}{120}N_5^i + \frac{y^4}{24}N_4^i + \frac{y^3}{6}N_3^i + \frac{y^2}{2}N_2^i + yc_4^i + c_5^i, \tag{8}$$

$$C = (b_1 + b_2 y)x + \frac{y^7}{1008}S_7 + \frac{y^6}{720}S_6 + \frac{y^5}{120}S_5 + \frac{y^4}{24}S_4 + \frac{y^3}{6}S_3 + \frac{y^2}{2}S_2 + yc_6^2 + c_7^2, \tag{9}$$

$$p_i' = \left[d_3^i\frac{y^2}{2} + d_2^i y + d_1^i\right]x + \frac{y^8}{8}K_8^i + \frac{y^7}{7}K_7^i + \frac{y^6}{6}K_6^i + \frac{y^5}{5}K_5^i + \frac{y^4}{4}K_4^i + \frac{y^3}{3}K_3^i + \frac{y^2}{2}K_2^i + yK_1^i + c_8^i. \tag{10}$$

The coefficients L_4^i, L_3^i, N_j^i, S_j and K_m^i ($i = 1, 2; j = 2, 7; m = 1, 8$) are expressed via the physical parameters of the problem: $g, \beta_i, \nu_i, \chi_i, \rho_i, D$ and γ, and the coefficients a_j^i and b_i ($i, j = 1, 2$) in the longitudinal temperature and concentration gradients are expressed as follows:

$$L_4^i = \frac{g\beta_i a_2^i}{\nu_i} + \delta_{2i}\frac{g\gamma b_2}{\nu_2}, \quad L_3^i = \frac{g\beta_i A}{\nu_i} + \delta_{2i}\frac{g\gamma b_1}{\nu_2},$$

$$N_7^1 = \frac{g\beta_1\left(a_2^1\right)^2}{\nu_1\chi_1}, \quad N_6^1 = 5\frac{g\beta_1 A a_2^1}{\nu_1\chi_1},$$

$$N_5^1 = \frac{1}{\chi_1}\left(\frac{g\beta_1(A)^2}{\nu_1} + 3a_2^1c_1^1\right), \quad N_4^1 = \frac{1}{\chi_1}\left(Ac_1^1 + 2a_2^1c_2^1\right),$$

$$N_3^1 = \frac{1}{\chi_1}\left(Ac_2^1 + a_2^1c_3^1\right), \quad N_2^1 = \frac{A}{\chi_1}c_3^1,$$

$$N_7^2 = B_2\frac{g}{\nu_2}\left(\beta_2 a_2^2 + \gamma b_2\right),$$

$$N_6^2 = B_1\frac{g}{\nu_2}\left(\beta_2 a_2^2 + \gamma b_2\right) + 4B_2\frac{g}{\nu_2}(\beta_2 A + \gamma b_1),$$

$$N_5^2 = B_1\frac{g}{\nu_2}(\beta_2 A + \gamma b_1) + 3B_2c_1^2,$$

$$N_4^2 = B_1c_1^2 + 2B_2c_2^2, \quad N_3^2 = B_1c_2^2 + B_2c_3^2, \quad N_2^2 = B_1c_3^2,$$

$$d_3^i = \rho_i g\beta_i a_2^i + \delta_{2i}\rho_2 g\gamma b_2,$$

$$d_2^i = \rho_i g\beta_i A + \delta_{2i}\rho_2 g\gamma b_1, \quad d_1^i = \rho_i\nu_i c_1^i,$$

$$S_7 = \frac{g}{\nu_2}\left(\beta_2 a_2^2 + \gamma b_2\right)E_2,$$

$$S_6 = \frac{g}{\nu_2}\left\{E_1\left(\beta_2 a_2^2 + \gamma b_2\right) + 4E_2(\beta_2 A + \gamma b_1)\right\},$$

$$S_5 = \frac{g}{\nu_2}(\beta_2 A + \gamma b_1)E_1 + 3E_2c_1^2, \quad S_4 = E_1c_1^2 + 2E_2c_2^2,$$

$$S_3 = E_1c_2^2 + E_2c_3^2, \quad S_2 = E_1c_3^2.$$

$$K_8^1 = \frac{1}{1008}\frac{\left(g\beta_1 a_2^1\right)^2\rho_1}{\nu_1\chi_1}, \quad K_7^1 = \frac{1}{144}\frac{(g\beta_1)^2\rho_1}{\nu_1\chi_1}Aa_2^1,$$

$$K_6^1 = \frac{1}{120}\frac{g\beta_1\rho_1}{\chi_1}\left(\frac{g\beta_1(A)^2}{\nu_1} + 3a_2^1c_1^1\right), \tag{11}$$

$$K_5^1 = \frac{1}{24}\frac{g\beta_1\rho_1}{\chi_1}\left(Ac_1^1 + 2a_2^1c_2^1\right),$$

$$K_4^1 = \frac{1}{6}\frac{g\beta_1\rho_1}{\chi_1}\left(Ac_2^1 + a_2^1c_3^1\right), \quad K_3^1 = \frac{1}{2}\frac{g\beta_1\rho_1}{\chi_1}Ac_3^1,$$

$$K_2^1 = g\beta_1\rho_1c_4^1, \quad K_1^1 = g\beta_1\rho_1c_5^1,$$

$$K_8^2 = \frac{1}{1008}\frac{\rho_2 g^2}{\nu_2}\left(\beta_2 a_2^2 + \gamma b_2\right)\left[B_2(\beta_2 - \alpha\gamma) + \frac{\gamma b_2}{D}\right],$$

$$K_7^2 = \frac{1}{720}\frac{\rho_2 g^2}{\nu_2}\left\{\left(\beta_2 a_2^2 + \gamma b_2\right)\left[B_1(\beta_2 - \alpha\gamma) + \frac{\gamma b_1}{D}\right] + 4(\beta_2 A + \gamma b_1)\left[B_2(\beta_2 - \alpha\gamma) + \frac{\gamma b_2}{D}\right]\right\},$$

$$K_6^2 = \frac{1}{120}\rho_2 g\left\{\frac{g}{\nu_2}(\beta_2 A + \gamma b_1) \times \left[B_1(\beta_2 - \alpha\gamma) + \frac{\gamma b_1}{D}\right] + 3\left[B_2(\beta_2 - \alpha\gamma) + \frac{\gamma b_2}{D}\right]c_1^2\right\},$$

$$K_5^2 = \frac{1}{24}\rho_2 g\left\{\left[B_1(\beta_2 - \alpha\gamma) + \frac{\gamma b_1}{D}\right]c_1^2 + 2\left[B_2(\beta_2 - \alpha\gamma) + \frac{\gamma b_2}{D}\right]c_2^2\right\},$$

$$K_4^2 = \frac{1}{6}\rho_2 g\left\{\left[B_1(\beta_2 - \alpha\gamma) + \frac{\gamma b_1}{D}\right]c_2^2 + \left[B_2(\beta_2 - \alpha\gamma) + \frac{\gamma b_2}{D}\right]c_3^2\right\},$$

$$K_3^2 = \frac{1}{2}\rho_2 g\left[B_1(\beta_2 - \alpha\gamma) + \frac{\gamma b_1}{D}\right]c_3^2,$$

$$K_2^2 = \rho_2 g\beta_2 c_4^2 + \rho_2 g\gamma c_6^2, \quad K_1^2 = \rho_2 g\beta_2 c_5^2 + \rho_2 g\gamma c_7^2.$$

Here, δ_{2i} is the Kronecker delta and B_1 and B_2 are determined from the following relations:

$$B_1 = \frac{DA - \chi_2\delta b_1}{D\chi_2(1-\alpha\delta)}, \quad B_2 = \frac{Da_2^2 - \chi_2\delta b_2}{D\chi_2(1-\alpha\delta)},$$
$$E_1 = \frac{b_1}{D} - \alpha B_1, \quad E_2 = \frac{b_2}{D} - \alpha B_2. \tag{12}$$

In formulas (11) and (12), the coefficients are calculated under the condition $a_1^1 = a_1^2 = A$ (see (5)), which follows from the continuity of temperature at the interface $y = 0$. The coefficients c_j^i ($i = 1, 2; j = 1, 8$) are constants of integration and will be found from the boundary conditions (see Sections 1.1 and 1.2).

1.1. Boundary Conditions in the Problem of a Two-Layer Flow with Allowance for Evaporation

Suppose that, on the lower ($y = -l$) and upper ($y = h$) solid impermeable channel walls (see Fig. 1), we have the no-slip boundary conditions (see also (6)):

$$u_1\big|_{y=-l} = 0, \quad u_2\big|_{y=h} = 0, \tag{13}$$

and the temperature linearly depends on the longitudinal coordinate:

$$T_1\big|_{y=-l} = A_1 x + \vartheta^-, \quad T_2\big|_{y=h} = A_2 x + \vartheta^+. \tag{14}$$

Let us consider two types of boundary conditions for the vapor concentration at the upper solid boundary $y = h$. In the first case, we assume the so-called total absorption of vapor,

$$C\big|_{y=h} = 0. \tag{15}$$

In the second case, we impose the absence of a vapor flux,

$$\left.\frac{\partial C}{\partial y}\right|_{y=h} = 0. \tag{16}$$

Let the gas flow in the upper layer be defined by the relationship

$$Q = \int_0^h \rho_2 u_2(y)dy. \tag{17}$$

At the thermocapillary interface, $y = 0$, we impose the conditions of continuity of the velocity and temperature:

$$u_1\big|_{y=0} = u_2\big|_{y=0}, \quad T_1\big|_{y=0} = T_2\big|_{y=0}. \tag{18}$$

At the thermocapillary interface, we also have the kinematic and dynamic conditions [23]. The first of them is satisfied automatically ($\upsilon_1\big|_{y=0} = 0, \upsilon_2\big|_{y=0} = 0$; see the form of exact solution (6)), and the dynamic conditions at the boundary $y = 0$ can be written as follows:

$$\rho_1\nu_1 u_{1y} = \rho_2\nu_2 u_{2y} + \sigma_T \left.\frac{\partial T_1}{\partial x}\right|_{y=0}, \quad p_1 = p_2. \tag{19}$$

Here, σ_T is the temperature coefficient of the surface tension, σ. We assume a linear dependence of the surface tension on temperature: $\sigma = \sigma_0 + \sigma_T(T - T_0)$, $\sigma_T = \text{const}$, and $\sigma_T < 0$. The balance of the heat flux is written with allowance for the diffusion mass flux of evaporating liquid at the interface (see [21, 23]):

$$\kappa_1 \frac{\partial T_1}{\partial y} - \kappa_2 \frac{\partial T_2}{\partial y} - \delta\kappa_2 \left.\frac{\partial C}{\partial y}\right|_{y=0} = -\lambda M. \tag{20}$$

Here, λ is the heat of evaporation, M is the mass rate ($M = \text{const}$) of evaporating liquid per unit area per unit time, and κ_1 and κ_2 are the thermal conductivities. The mass balance equation with allowance for thermal diffusion at the interface has the following form [19, 21, 23]):

$$M = -D\rho_2 \left(\left.\frac{\partial C}{\partial y}\right|_{y=0} + \alpha \left.\frac{\partial T_2}{\partial y}\right|_{y=0} \right). \tag{21}$$

The concentration of saturated vapor at the interface will be determined by the relationship

$$C\big|_{y=0} = C_* \left[1 + \varepsilon\left(T_2\big|_{y=0} - T_0\right)\right], \tag{22}$$

which follows from Clapeyron–Clausius equation $P = P_0 \exp[(\lambda\mu/R)(1/T_0 - 1/T)]$ and the Mendeleev–Clapeyron equation $\rho_\upsilon RT = \mu P$ for an ideal gas ((P_0, T_0) is an initial state, $\rho_\upsilon = C\rho_2$) [35]. Equation (22) was under the condition that the parameter εT_* for moderate variations in temperature is small [18, 21, 36]. Here, T_0 is an initial temperature, C_* is the concentration of saturated vapor at $T_2 = T_0$ (T_0 is 20°C, as in [19, 21]), $\varepsilon T_* = \lambda\mu/(RT_0^2)$, μ is the molar mass of the evaporating liquid, R is the universal gas constant, and T_* is the characteristic temperature drop. It should be noted that Eqs. (1)–(5) and boundary conditions (13)–(22) admit a replacement of the unknown functions T_i by $(T_i - T_0)$; then, we can assume the condition

$$C\big|_{y=0} = C_* \left[1 + \varepsilon T_2\big|_{y=0}\right], \tag{23}$$

as the condition used in [19] (see also [21]). If the algorithm for calculating the integration constants will be implemented with condition (23), then the problem will reduce to finding the temperature function of the form $(T - T_0)$.

Note that the exact equation for the mass balance of vapor [10] requires that the coefficient D in Eq. (21) be divided by $(1 - C)$ (see also [37, 38]). The conditions of smallness of the parameter $(C_*\varepsilon T_*)$ make it possible to calculate the mass evaporation rate M according to (21), where D is understood as the reduced diffusion coefficient and is the diffusion coefficient divided by $(1 - C_*)$.

1.2. Determining the Unknown Coefficient in the Case of Boundary Conditions (15) for Vapor Concentration at the Upper Boundary

Suppose that the concentration C at the upper boundary of the channel satisfied condition (15). Condition (15) of zero vapor concentration can be explained by the ability of the boundary to instantly absorb vapor (i.e., the property of complete vapor absorption [19]). For real physical situations, on condensation or freezing out of vapor, the boundary value of C at the upper solid wall can vary as a function of temperature.

Taking into account the thermodiffusion effect in the gas–vapor layer, from condition (15),

$$b_2 = -b_1/h, \quad \varphi(h) = 0. \tag{24}$$

Taking into account the form of solution (6) and the condition (18) of continuity of temperature at the interface, we find that the coefficients a_1^1 and a_1^2 are the same: (which is taken into account in (11): A = const). Conditions (18) of the continuity of the velocity and temperature at the boundary $y = 0$ imply the equalities

$$c_3^1 = c_3^2, \quad c_5^1 = c_5^2. \tag{25}$$

Equations (22) (or (23)) for the saturated vapor concentration imply

$$b_1 = C_*\varepsilon A, \quad c_7^2 = C_* + C_*\varepsilon\left(c_5^2 - T_0\right). \tag{26}$$

Then, coefficient b_2 entering into the longitudinal concentration gradient is determined from the expression $b_2 = -C_*\varepsilon A/h$ (see (24) and (26)). Due to the linear temperature distribution (14) over the longitudinal coordinate at the solid boundaries, we have the equalities

$$a_2^1 = (A - A_1)/l, \quad a_2^2 = (A_2 - A)/h, \tag{27}$$

and

$$\vartheta_1(-l) = \vartheta^-, \quad \vartheta_2(h) = \vartheta^+. \tag{28}$$

Mass balance equation (21) dictates the relationships

$$b_2 = -\alpha a_2^2, \quad M = -D\rho_2\left(c_6^2 + \alpha c_4^2\right). \tag{29}$$

Hence, the longitudinal temperature gradients at the upper boundary and the interface are related as follows: $A_2 = A + C_*\varepsilon A/\alpha$. Heat transfer condition (20) at the interface requires that

$$\begin{aligned} \kappa_1 a_2^1 - \kappa_2 a_2^2 - \delta\kappa_2 b_2 = 0, \\ \kappa_1 c_4^1 - \kappa_2 c_4^2 - \delta\kappa_2 c_6^2 = -\lambda M. \end{aligned} \tag{30}$$

Then, from (27) and the first equations in (29) and (30), we determine the interdependence of the gradients A and A_1. Thus, we have established the relationship between the longitudinal temperature gradients A, A_1, and A_2 that should be maintained at the channel boundaries:

$$\begin{aligned} A_2 = A + C_*\varepsilon A/\alpha, \\ A_1 = A + A(l/h)(\kappa_2/\kappa_1)(C_*\varepsilon/\alpha)(\alpha\delta - 1). \end{aligned} \tag{31}$$

Dynamic conditions (19) imply the expressions

$$\begin{aligned} c_1^1 = c_1^2\,\rho_2\nu_2/(\rho_1\nu_1), \\ c_2^1 = c_2^2\,\rho_2\nu_2/(\rho_1\nu_1) + \sigma_T A/(\rho_1\nu_1). \end{aligned} \tag{32}$$

From the second equations in (29) and (30), we have the following relationships between the integration constants c_6^2, c_4^1, and c_4^2:

$$\begin{aligned} c_6^2 = c_4^1\,\kappa_1/(\lambda D\rho_2 + \delta\kappa_2) \\ - c_4^2\,(\kappa_2 + \lambda D\rho_2\alpha)/(\lambda D\rho_2 + \delta\kappa_2). \end{aligned} \tag{33}$$

The integration constants c_1^2, c_2^2, and c_3^2 are defined as the solutions of a system of linear algebraic equations dictated by no-slip conditions (13) at the boundaries $y = -l$ and $y = h$ and specified gas flow rate (17) in the upper layer:

$$\begin{aligned} \frac{l^2}{2}\frac{\rho_2\nu_2}{\rho_1\nu_1}c_1^2 - l\frac{\rho_2\nu_2}{\rho_1\nu_1}c_2^2 + c_3^2 \\ = \frac{\sigma_T A l}{\rho_1\nu_1} - \frac{g\beta_1}{\nu_1}\left(a_2^1\frac{l^4}{24} - A\frac{l^3}{6}\right), \\ \frac{h^2}{2}c_1^2 + hc_2^2 + c_3^2 \\ = -\frac{g}{\nu_2}\left[\frac{h^4}{24}\left(\beta_2 a_2^2 + \gamma b_2\right) + \frac{h^3}{6}\left(\beta_2 A + \gamma b_1\right)\right], \\ \frac{h^3}{6}c_1^2 + \frac{h^2}{2}c_2^2 + hc_3^2 \\ = \frac{Q}{\rho_2} - \frac{g}{\nu_2}\left[\frac{h^5}{120}\left(\beta_2 a_2^2 + \gamma b_2\right) + \frac{h^4}{24}\left(\beta_2 A + \gamma b_1\right)\right]. \end{aligned} \tag{34}$$

Taking into account the second conditions in (25) and (26) and the relationship between constants (33), we can determine the unknown c_4^1, c_4^2, and c_5^1 from the following system of equations dictated by the conditions for the temperature and concentration (see the second condition in (24) and relation (28)):

$$\begin{aligned} -lc_4^1 + c_5^1 = \vartheta^- + \frac{l^7}{1008}\frac{g\beta_1(a_2^1)^2}{\nu_1\chi_1} \\ - \frac{l^6}{144}\frac{gA\beta_1 a_2^1}{\nu_1\chi_1} + \frac{l^5}{120}\left(\frac{g\beta_1(A)^2}{\nu_1\chi_1} + \frac{3a_2^1}{\chi_1}c_1^1\right) \\ - \frac{l^4}{24}\left(\frac{A}{\chi_1}c_1^1 + \frac{2a_2^1}{\chi_1}c_2^1\right) + \frac{l^3}{6}\left(\frac{A}{\chi_1}c_2^1 + \frac{a_2^1}{\chi_1}c_3^1\right) - \frac{l^2}{2}\frac{A}{\chi_1}c_3^1, \end{aligned}$$

$$
\begin{aligned}
hc_4^2 + c_5^1 &= \vartheta^+ - \frac{h^7}{1008}\frac{g}{\nu_2}B_2\left(\beta_2 a_2^2 + \gamma b_2\right) \\
&- \frac{h^6}{720}\frac{g}{\nu_2}\left[B_1\left(\beta_2 a_2^2 + \gamma b_2\right) + 4B_2\left(\beta_2 A + \gamma b_1\right)\right] \\
&- \frac{h^5}{120}\left[\frac{g}{\nu_2}B_1\left(\beta_2 A + \gamma b_1\right) + 3B_2 c_1^2\right] \\
&- \frac{h^4}{24}\left[B_1 c_1^2 + 2B_2 c_2^2\right] - \frac{h^3}{6}\left[B_1 c_2^2 + B_2 c_3^2\right] - \frac{h^2}{2}B_1 c_3^2,
\end{aligned} \tag{35}
$$

$$
\begin{aligned}
h\frac{\kappa_1}{D\rho_2\lambda + \delta\kappa_2}c_4^1 - h\frac{\lambda D\rho_2\alpha + \kappa_2}{D\rho_2\lambda + \delta\kappa_2}c_4^2 + C_*\varepsilon c_5^1 \\
= -\frac{h^7}{1008}\frac{g}{\nu_2}E_2\left(\beta_2 a_2^2 + \gamma b_2\right) \\
- \frac{h^6}{720}\frac{g}{\nu_2}\left[E_1\left(\beta_2 a_2^2 + \gamma b_2\right) + 4E_2\left(\beta_2 A + \gamma b_1\right)\right] \\
- \frac{h^5}{120}\left[\frac{g}{\nu_2}E_1\left(\beta_2 A + \gamma b_1\right) + 3E_2 c_1^2\right] \\
- \frac{h^4}{24}\left[E_1 c_1^2 + 2E_2 c_2^2\right] - \frac{h^3}{6}\left[E_1 c_2^2 + E_2 c_3^2\right] \\
- \frac{h^2}{2}E_1 c_3^2 - C_* + C_*\varepsilon T_0.
\end{aligned}
$$

For known values of c_1^2, c_2^2, c_3^2, c_4^1, c_4^2, and c_5^1, the integration constants c_1^1, c_2^1, c_3^1, and c_5^2 are determined from (25) and (32). For determining c_6^2, we have relationship (33), and the integration constant c_7^2 can be found with the help of condition (26) if c_5^1 is known.

If all the integration constants are known, the mass rate M of the liquid evaporating from the interface is determined from, e.g., the second relationship (29).

If we neglect the Soret effect in the upper layer of the system, then mass balance condition (21) and boundary condition (15) for the vapor concentration will necessitate setting to zero the coefficient determining the temperature gradient along the interface: $A = 0$. Thus, the simulation of two-layer steady-state flows reduces to fluid flows with a liquid–liquid interface $y = 0$. In this case, the vapor concentration in the gas layer will be independent of the longitudinal coordinate, since $b_1 = 0$ and $b_2 = 0$ (see the first relationships in (24) and (26)). From the condition of heat transfer at the interface (see the first equality in (30)), it follows that we must impose longitudinal temperature gradients at the upper and lower hard walls of the channel, satisfying the relationship

$$A_2 = -A_1(h/l)(\kappa_1/\kappa_2). \tag{36}$$

In this case, we have $a_2^1 = -A_1/l$ and $a_2^2 = A_2/h$ (see (27) for $A = 0$). As a result, the unknown integration constants c_1^2, c_2^2, c_3^2 and c_4^1, c_4^2, c_5^1 will be determined from the systems of linear algebraic equations (34) and (35) in which we must take into account the aforementioned values of the temperature and concentration gradients (A, a_2^1, a_2^2, b_1, b_2), the dependence of A_2 of form (36), and the value $\alpha = 0$.

1.3. Determining the Unknown Coefficient in the Case of Boundary Conditions (16) for the Vapor Concentration at the Upper Boundary

Suppose that the Soret effect is taken into account in the formulation of problem (1)–(22). If, at the upper wall of the channel, we impose condition (16) of zero vapor flux (see, e.g., [17, 37, 38] and also [21]), then we will have the equalities

$$b_2 = 0, \quad \varphi'(h) = 0, \tag{37}$$

which follow from this condition (here, the prime denotes the derivative with respect to y). Conditions (18) of the continuity of the velocity and temperature at the thermocapillary boundary $y = 0$ require that equality (25) be satisfied. From conditions (14) of the linear temperature distribution at the solid boundaries $y = -l$ and $y = h$, we have equalities similar to (27) and (28). Mass balance condition (21) leads to relationships (29), the first of which, with allowance for (37), implies that

$$a_2^2 = 0. \tag{38}$$

Heat transfer condition (20) at the interface $y = 0$ imply Eqs. (30). From the first equation in (30), the equality

$$a_2^1 = 0, \tag{39}$$

since we have (38) and the first of conditions (37). From (27), (38), and (39), it follows that the longitudinal temperature gradients at the solid and free boundaries are the same:

$$A = A_1 = A_2. \tag{40}$$

The equation for the saturated vapor concentration in form (22) implies relationship (26). Dynamical conditions (19) lead to equalities (32), relating the constants of integration c_1^1 and c_1^2 as well as c_2^1 and c_2^2.

Taking into account the reasoning above, we have a system of equations for determining the unknown constants c_1^2, c_2^2, and c_3^2 from no-slip conditions (13) and expression (17), determining the gas flow in the upper layer of the channel. Taking into account formulas (25) and (32), we also have

$$
\begin{aligned}
\frac{l^2}{2}\frac{\rho_2\nu_2}{\rho_1\nu_1}c_1^2 - l\frac{\rho_2\nu_2}{\rho_1\nu_1}c_2^2 + c_3^2 &= \frac{l^3}{6}\frac{g\beta_1 A}{\nu_1} + \frac{\sigma_T A l}{\rho_1\nu_1}, \\
\frac{h^2}{2}c_1^2 + hc_2^2 + c_3^2 &= -\frac{h^3}{6}\frac{g}{\nu_2}\left(\beta_2 A + \gamma b_1\right),
\end{aligned}
$$

$$\frac{h^3}{6}c_1^2 + \frac{h^2}{2}c_2^2 + hc_3^2 = \frac{Q}{\rho_2} - \frac{h^4}{24}\frac{g}{\nu_2}(\beta_2 A + \gamma b_1).$$

With the c_1^2, c_2^2, and c_3^2 found, we determine c_1^1, c_2^1, and c_3^1 from (25) and (32). With (37)–(39), the second relationship (37) determines the constant of integration

$$c_6^2 = -\frac{h^4}{24}\frac{g}{\nu_2}(\beta_2 A + \gamma b_1) E_1 - \frac{h^3}{6} E_1 c_1^2 - \frac{h^2}{2} E_1 c_2^2 - h E_1 c_3^2.$$

The constants c_4^1 and c_5^1 are found from the system of equations (28):

$$-lc_4^1 + c_5^1 = \vartheta^- + \frac{l^5}{120}\frac{g\beta_1 (A)^2}{\nu_1 \chi_1} - \frac{l^4}{24}\frac{A}{\chi_1}c_1^1 + \frac{l^3}{6}\frac{A}{\chi_1}c_2^1 - \frac{l^2}{2}\frac{A}{\chi_1}c_3^1,$$

$$h\frac{\kappa_1}{\kappa_2 + \lambda D \rho_2 \alpha}c_4^1 + c_5^1 = \vartheta^+ - \frac{h^5}{120}\frac{g}{\nu_2} B_1 (\beta_2 A + \gamma b_1) - \frac{h^4}{24} B_1 c_1^2 - \frac{h^3}{6} B_1 c_2^2 - \frac{h^2}{2} B_1 c_3^2 + h\frac{\delta\kappa_2 + \lambda D \rho_2}{\kappa_2 + \lambda D \rho_2 \alpha}c_6^2.$$

For calculating E_1 and B_1, see (12). Note that the second relationships in (30) and (29) were used for the equation determining the integration constant c_4^2:

$$c_4^2 = c_4^1 \frac{\kappa_1}{\kappa_2 + \lambda D \rho_2 \alpha} - c_6^2 \frac{\delta\kappa_2 + \lambda D \rho_2}{\kappa_2 + \lambda D \rho_2 \alpha},$$

but c_7^2 is found using the second formula in (26). The mass rate M of liquid evaporating from the interface can be found, e.g., with the help of the second equation in (29).

If the Soret effect is not taken into account in the simulation, the condition of zero vapor flux (16) leads to equalities (37), and the conditions providing the thermal regime at the channel boundaries (see (27) and the first relation in (30)) imply the dependence of the longitudinal gradient A_2 on A and A_1:

$$A_2 = A + (A - A_1)(h/l)(\kappa_1/\kappa_2). \quad (41)$$

Note that two of the three longitudinal temperature gradients at the channel boundaries can be considered specified (a_2^1 and a_2^2 calculated according to (27)). Equation (22) dictates the fulfillment of relationship (26) and determines the coefficient b_1, and dynamic conditions (19) and continuity conditions (18) require the fulfillment of equalities (32) and (25) and determine the relationships between c_1^2, c_2^2, c_3^2, c_1^1, c_2^1, c_3^1, c_5^1, and c_5^2. With the above reasoning, the system of equations for the unknown c_1^2, c_2^2, and c_3^2 follows from conditions (13) and (17). With the known c_1^2, c_2^2, and c_3^2, the integration constant c_6^2 is determined from the second condition in (37). Then, from the second relation (29) written at $\alpha = 0$, we immediately find the mass rate M of the liquid evaporating from the interface. Constants c_4^1 and c_5^1 are found from a system of linear algebraic equations following from conditions (28) for the temperature at the solid boundaries of the channel.

Thus, we can be determine all unknown integration constants c_j^i ($i = 1, 2; j = 1, ..., 7$), construct the exact solutions (u_i, p_i', T_i, C) satisfying Eqs. (1)–(5) and boundary conditions (13)–(22), and find the mass evaporation rate M.

2. RESULTS OF ANALYTICAL CALCULATIONS AND COMPARISON WITH EXPERIMENTS

Let us consider an HFE-7100–nitrogen liquid–gas system. The fluid for the study was HFE-7100 due to its physicochemical properties. HFE-7100 belongs to the class of hydroesters and has the following properties: volatile (boiling point of –61°C); low surface tension (13.6 mN/m); dielectric; a low global warming potential; zero ozone depletion potential; compatible with most metals, plastics, elastomers, etc. This liquid is used in various industries as a coolant in thermostabilization and cooling systems. HFE-7100 is accepted as a working fluid for a number of space experiments [39, 40] under zero gravity conditions aboard the International Space Station, because it meets the necessary properties and is nonflammable, nontoxic, and safe. The properties and detailed description of the liquid are presented in the manufacturer's website [41] and in [6, 42]. The upper layer of the channel is filled with nitrogen. The main physical parameters of the system are as follows (see [6, 20, 25, 42, 43]): $\rho_1 = 1.4\times10^3$ kg/m^3 and $\rho_2 = 1.2$ kg/m^3 are the density of liquid and gas; $\nu_1 = 0.38\times10^{-6}$ m^2/s and $\nu_2 = 0.15\times10^{-4}$ m^2/s are the kinematic viscosities; $\chi_1 = 0.3\times10^{-4}$ m^2/s and $\chi_2 = 0.4\times10^{-7}$ m^2/s are the thermal diffusivities; $\kappa_1 = 0.07$ W/(m K) and $\kappa_2 = 0.0251$ W/(m K) are the thermal conductivities; $\beta_1 = 1.8\times10^{-3}$ K^{-1} and $\beta_2 = 3.37\times10^{-3}$ K^{-1} are the coefficients of thermal expansion of the liquid and gas; $\gamma = -0.62$ is the concentration density coefficient (see [19], but for the gasoline–air pair); $\varepsilon = 0.04$ (K^{-1}); $C_* = 0.7$ (see (22)), if $T_0 = 20^\circ$C, is the temperature coefficient of surface tension; $\sigma_T = -1.5\times10^{-5}$ (N/(m K)) is the temperature coefficient of surface tension; and $D = 2\times10^{-5}$ (m^2/s) is the vapor diffusion coefficient

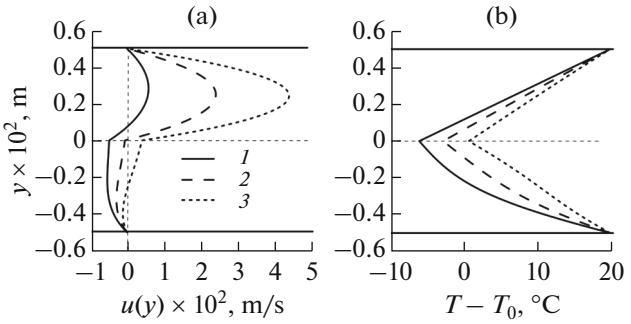

Fig. 2. Velocity (a) and (b) temperature profiles in an HFE-7100–nitrogen system at $h = 0.5 \times 10^{-2}$ m, $l = 0.5 \times 10^{-2}$ m, $A_1 = -30$ K/m, and different gas flow rates in the upper layer without taking into account the Soret effect: $Q = (1)$ 1.8×10^{-5}, (2) 9.6×10^{-5}, and (3) 1.8×10^{-4} kg/(m s); $A = 0$ K/m; and $A_2 = 82.5$ K/m.

in the upper layer. The Dufour and Soret coefficients are set to $\delta = 10^{-3}$ and $\alpha = 5 \times 10^{-3}$ and -5×10^{-4} (in the case of normal thermal diffusion, possible values of these coefficients can be found in [23]; see also references therein).

Experimental measurements were carried out at a test bench for the study of convection caused by intensive evaporation of liquid in a horizontal cell of limited size under the action of a gas flow [5, 6]. Between the cell with a liquid (length of 40 mm and width of 40 mm) and a gas channel (width of 100 mm and height of 5 mm), a separation plate with a thickness of 200 μm was installed. This plate has a square cut (10 × 10 mm) at the center, where the liquid and gas come into contact. The flow rate of the liquid (HFE-7100) varied from 40 to 350 μL/min, which corresponds to a mass evaporation rate of 0.014 to 0.11 kg/m^2 s. The gas flow rate (nitrogen, 99.8%) varied from 0.1 to 5 L/min. The Reynolds number varied in the range 40–200, which corresponds to a mean gas velocity of 0.014 to 0.24 m/s. The temperature of the liquid and gas varied from 20 to 40°C and higher, and the thickness of the liquid layer varied from 1.5 to 8 mm.

2.1. The Influence of the Soret Effect on the Flow Structure and Temperature and Vapor Concentration Distributions in the System

Figures 2a and 3b show velocity (Figs. 2a, 3a), temperature (Figs. 2b, 3b), and concentration (Fig. 3c) profiles without and with taking into account the thermodiffusion effect in the gas–vapor layer for different gas flow rates in the upper layer, calculated by analytical formulas. The calculations were performed for the vapor absorption condition problem (15) at the upper solid wall of the channel, the longitudinal temperature gradient $A_1 = -30$ K/m specified at the bottom wall; the height of the gas layer, h; and liquid layer, l, of 0.5×10^{-2} m. In both cases, both with and without the Soret effect, an increase in the gas flow entails an increase in the fluid flow intensity (Figs. 2a, 3a). The velocity profiles have a similar character (see Figs. 2a, 3a), but there are some qualitative and quantitative differences. In particular, if the thermodiffusion effect is disregarded (Fig. 2a), the velocity U at the interface $y = 0$ takes the value of -0.48×10^{-2} m/s at a gas flow Q of 1.8×10^{-5} kg/(m s). At $Q = 9.6 \times 10^{-5}$ kg/(m s), this quantity reaches a value of -5.5×10^{-4} m/s. Thus, at the given gas flow rates, in the liquid layer, a flow in the direction opposite to the gas flow is observed. With an increase in gas flow rate, at $Q = 1.8 \times 10^{-4}$ kg/(m s), the velocity U at the interface is 4.04×10^{-2} m/s. If the Soret effect is taken into account and the thermal diffusion coefficient is $\alpha = -5 \times 10^{-3}$, the velocity U for the same gas flow rates (1.8×10^{-5}, 9.6×10^{-5}, and 1.8×10^{-4} kg/(m s)) reaches the values of 0.68×10^{-3}, 0.5×10^{-2}, and 0.95×10^{-2} m/s, respectively. Thus, in the case when the effect of thermal diffusion is taken into account, there is no reverse flow and a stratification of the flow takes place (see Fig. 3a). The temperature distribution with a variation in Q qualitatively

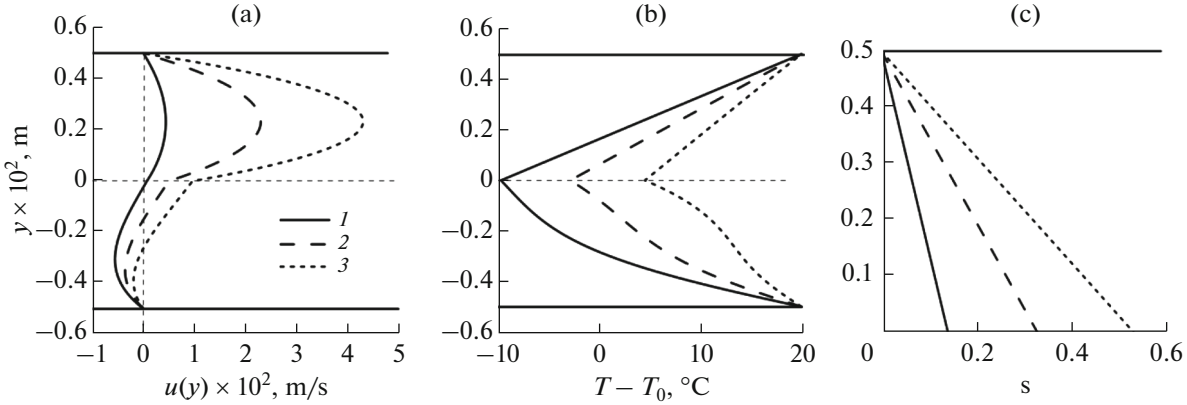

Fig. 3. Velocity (a), temperature (b), and (c) concentration profiles in an HFE-7100–nitrogen system with allowance for the Soret effect: (1) $Q = 1.8 \times 10^{-5}$, (2) 9.6×10^{-5}, and (3) 1.8×10^{-4} kg/(m s); $A = -9.88$ K/m; $A_2 = 45.5$ K/m; and $\alpha = -5 \times 10^{-3}$.

changes (Fig. 2b, 3b). In the upper layer, the nonlinearity of the temperature distribution is rather weak both with and without taking into account the Soret effect. In the liquid (the lower layer in Figs. 2b, 3b), the nonlinearity is stronger when the effect of thermodiffusion is taken into account (Fig. 3b) than when it is disregarded. With an increase in the gas flow rate, the vapor concentration at the boundary $y = 0$ increases (Fig. 3c). This effect can be caused by the intensification of convective heat transfer between warmer gas and the cold interface. It should be noted that, at any gas flow rate, the temperature at the interface is significantly lower than the temperature imposed at the solid channel walls. A qualitatively similar effect is observed in the experiments [5, 6].

2.2. The Influence of the Thickness of the Liquid Layer on the Flow Structure, Temperature Distribution, and Vapor Concentration in the System

The thickness of the liquid layer, l, has a strong effect on the velocity profiles, the temperature distribution, and the vapor concentration. For example, if the Soret effect is taken into account, for $l = 0.5 \times 10^{-2}$ m, the reverse currents in the lower layer are observed (Fig. 3a), while, for $l = 0.15 \times 10^{-2}$ m, the fluid motion is unidirectional and the fluid moves only in the direction of the gas flow (Fig. 4a). Significant qualitative and quantitative differences in the temperature profiles are observed for different values of the liquid layer thickness l. For small thicknesses l (see Fig. 4b), the nonlinearity in the temperature distribution is rather weak and the temperature distribution in the system is close to linear. With increasing thickness l of the lower layer, the nonlinearity of the temperature profile becomes more pronounced (Fig. 3b); the variation in the gas flow rate in this case has a significantly stronger effect on the temperature profiles, the interface $y = 0$ is heated more intensively but remains colder than in the two-layer system with a smaller thickness l (see Figs. 3b, 4b). The analysis of the vapor concentration distribution in the gaseous medium has shown that, for $l = 0.15 \times 10^{-2}$ m, higher concentrations at the boundary $y = 0$ are achieved than for $l = 0.5 \times 10^{-2}$ m. In particular, at $Q = 1.8 \times 10^{-5}$ if the thickness of the liquid layer is $l = 0.5 \times 10^{-2}$ m, the vapor concentration at the boundary $y = 0$ reaches 0.14 and, if $l = 0.15 \times 10^{-2}$ m, the vapor concentration is 0.59. For $Q = 9.6 \times 10^{-5}$ kg/(m s), we have $C|_{y=0} = 0.33$ for $l = 0.5 \times 10^{-2}$ m and, $C|_{y=0} = 0.60$, for $l = 0.15 \times 10^{-2}$ m. At the maximum value of gas flow rate, $Q = 1.8 \times 10^{-4}$ kg/(m s), for the thickness of the liquid layer $l = 0.5 \times 10^{-2}$ m, we have $C|_{y=0} = 0.54$, and for $l = 0.15 \times 10^{-2}$ m, the vapor concentration at the interface is $C|_{y=0} = 0.61$. It should also be noted that variation in the gas flow rate has smaller effect on the concentration profiles at a smaller layer thickness $l = 0.15 \times 10^{-2}$ m than at a thickness of 0.5×10^{-2} m.

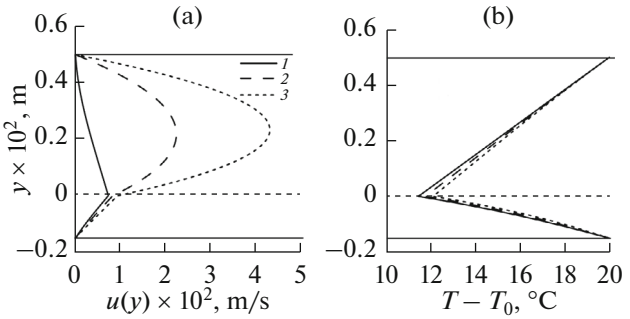

Fig. 4. (a) Velocity and (b) temperature profiles in an HFE-7100–nitrogen system at $h = 0.5 \times 10^{-2}$ m, $l = 0.15 \times 10^{-2}$ m, $A_1 = -30$ K/m, and different gas flow rates in the upper layer with allowance for the Soret effect: $Q = (1)$ 1.8×10^{-5}, (2) 9.6×10^{-5}, and (3) 1.8×10^{-4} kg/(m s); $A = -18.6$ K/m; and $A_2 = 85.66$ K/m.

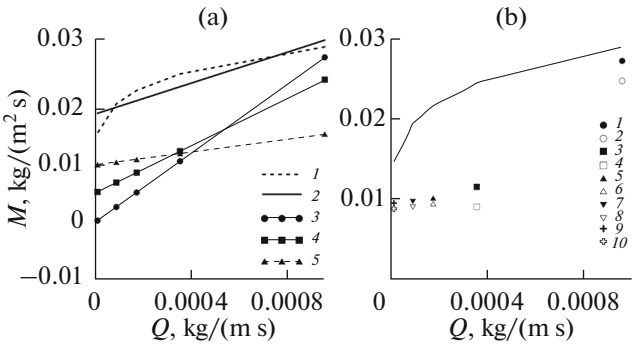

Fig. 5. Evaporation rate of fluid vs. gas flow rate, $h = 0.5 \times 10^{-2}$ m, $l = 0.5 \times 10^{-2}$ m: (a) (1) experimental data, (2) trend line of experimental data, and (3–5) calculations for $A_1 = -80$, -55, and -15 K/m, respectively; (b) (solid line) approximation of experimental data (Table 1) and (dots)theoretical results: (1) $M = 2.7 \times 10^{-2}$ kg/(m^2 s), $A_1 = -80$ K/m; (2) $M = 2.45 \times 10^{-2}$, $A_1 = -80$; (3) $M = 1.14 \times 10^{-2}$, $A_1 = -55$; (4) $M = 0.9 \times 10^{-2}$, $A_1 = -55$; (5) $M = 1.01 \times 10^{-2}$, $A_1 = -15$; (6) $M = 0.94 \times 10^{-2}$, $A_1 = -15$; (7) $M = 0.96 \times 10^{-2}$, $A_1 = -10$; (8) $M = 0.89 \times 10^{-2}$, $A_1 = -10$; (9) $M = 0.94 \times 10^{-2}$; $A_1 = -3$; (10) $M = 0.87 \times 10^{-2}$, $A_1 = -3$.

2.3. The Influence of the Gas Flow Rate on the Evaporation Rate

The comparison of the experimental and analytical results on the dependence of the amount of evaporated liquid (or the mass evaporation rate M) on the gas flow rate Q at the interface has shown that, although these results have qualitatively the same character (an increase in M with an increase in Q), they differ quantitatively. The experimental dependence of M on Q is nonlinear (see *1* in Fig. 5a), while analytical calculations give a linear dependence (*3–5* in Fig. 5a). Of course, the analytical calculations carried out for the two-dimensional case do not take into account all factors present in the experiment. To compare the exper-

Table 1

Q, kg/(m s)	M, kg/(m^2 s), experiment	M, kg/(m^2 s), theory
9.6×10^{-4}	2.873×10^{-2}	2.7×10^{-2}
3.6×10^{-4}	2.425×10^{-2}	1.14×10^{-2}
1.8×10^{-4}	2.151×10^{-2}	1.01×10^{-2}
9.6×10^{-5}	1.929×10^{-2}	9.62×10^{-3}
1.8×10^{-5}	1.444×10^{-2}	9.43×10^{-3}

imental results with the analytical calculations, we use a linear approximation of the experimental data (*2* in Fig. 5a). From the graphs shown in Fig. 5a and the values shown in Fig. 5b and in Table 1, it is clear that there exist the values of the longitudinal temperature gradient at which the experimental and analytical results are close both quantitatively (Table 1) and qualitatively (Fig. 5). Thus, for a longitudinal temperature gradient at the lower solid boundary of $A_1 = -55$ K/m, the difference between the values of the evaporation rate is within a factor of two and the slope of the line is close to the slope of the trend line (linear approximation) of the experimental data (see Fig. 5a, *1* and *4*). For the longitudinal temperature gradient at the lower solid boundary of $A_1 = -80$ K/m, for the maximum values of the gas flow rate Q in the upper layer ($Q = 9.6 \times 10^{-4}$ kg/(m s)), the analytical calculations give the value of the mass evaporation rate M closest to the experimental value ($M = 2.7 \times 10^{-2}$ kg/(m^2 s), $A_1 = -80$ K/m, $A = -20.47$ K/m, and $A_2 = 143.26$ K/m). Table 1 presents the comparison of the evaporation rate from the interface, in the physical experiments (the second column) and calculated analytically for different values of the longitudinal temperature gradients and gas flow rate in the upper layer (third column). For $Q = 3.6 \times 10^{-4}$ kg/(m s), the value of $M = 1.14 \times 10^{-2}$ kg/(m^2 s) is reached at $A_1 = -55$ K/m (here, $A = -14.07$ K/m, $A_2 = 98.49$ K/m). At $Q = 1.8 \times 10^{-4}$ kg/(m s), the value of $M = 1.01 \times 10^{-2}$ kg/(m^2 s) was at $A_1 = -15$ K/m ($A = -3.84$ K/m, $A_2 = 26.86$ K/m). At a gas flow rate of $Q = 9.6 \times 10^{-5}$ kg/(m s), the mass evaporation rate $M = 9.62 \times 10^{-3}$ kg/(m^2 s) is reached at $A_1 = -10$ K/m ($A = -2.56$ K/m, $A_2 = 17.91$ K/m) and, at $Q = 1.8 \times 10^{-5}$ kg/(m s), the value of $M = 9.43 \times 10^{-3}$ kg/(m^2 s) was at $A_1 = -3$ K/m ($A = -0.77$ K/m, $A_2 = 5.37$ K/m). It should be noted that, due to inhomogeneous evaporation, the values of the longitudinal temperature gradients on the order of 3–80 K/m, used in analytical calculations, are quite realistic for the experiment [6]. However, better agreement between the analytical results and the experimental data (Table 1) can be achieved at higher values of T_0 (see (22); $T_0 = 60$°C) and, accordingly, greater values of ϑ^+ and ϑ^- (see (14); ϑ^+ and ϑ^- vary in the range of 40–80°C).

An increase in the transverse temperature drop (here, $|\vartheta^+ - \vartheta^-|$) leads to an increase in the evaporation rate M in analytical calculations (Fig. 5b). All calculations were performed for the experimental values of the gas flow rate Q (see Table 1, first column).

CONCLUSIONS

The results of mathematical modeling of steady-state two-layer flows based on the exact solutions of the Navier–Stokes equations in the Boussinesq approximation were presented. The solutions were constructed with allowance for the evaporation at the interface and thermodiffusion and diffusion thermal conductivity in the upper layer of the system. Note that it is the exact solutions that enable one to analyze the adequacy of the formulation of a mathematical model of two-layer fluid flows with an interface and to reveal significant factors influencing the flow characteristics. It turned out that taking into account the Soret effect allows one to consider an interface as a thermocapillary surface in the case when the upper wall of the channel can absorb vapor. If, on the upper solid boundary of the flow region, a condition typical of vapor absorption is imposed and the Soret effect is disregarded, then, when simulating two-layer flows of form (6), it is necessary to set to zero the longitudinal temperature gradient A at the interface. When the thermodiffusion effect is taken into account, the boundary value of one of the longitudinal temperature gradients determines the values of the other two through specific coupling conditions (see (31)). Under the condition of a zero-vapor flux at the upper solid channel wall, the simulation of two-layer flows is performed at a given longitudinal gradient of temperature, the same for all channel boundaries, if the Soret effect is taken into account (see condition (40)). If the Soret effect is not taken into account in the simulation in the absence of the vapor flow at the upper boundary, then two of the three longitudinal temperature gradients at the channel boundaries can be considered specified (see (41)). Thus, the Soret effect changes the flow quantitatively and qualitatively, and enables one to change the mechanism of control of the flow pattern by specifying longitudinal temperature gradients at the channel boundaries and matching their values.

Examples of velocity, temperature, and concentration profiles for the HFE-7100–nitrogen liquid–gas system were presented for different values of gas flow in the upper layer with and without taking into account the Soret effect for different thicknesses of the liquid layer. The analytical and experimental results on the evaporation mass rate M of liquid on the thermocapillary interface as a function of the gas flow rate and longitudinal temperature gradients were compared. The qualitative and, in some cases, quantitative agreement between them was revealed.

ACKNOWLEDGMENTS

This work was supported by the Russian Foundation for Basic Research, project no. 14-08-00163, and the Russian Science Foundation, project no. 14-19-01755.

REFERENCES

1. Scheid, B., Margerit, J., Iorio, C.S., Joannes, L., Heraud, M., Queeckers, P., Dauby, P.C., and Colinet, P., *Exp. Fluids*, 2012, vol. 52, p. 1107.
2. Kabov, O.A., Zaitsev, D.V., Cheverda, V.V., and Bar-Cohen, A., *Exp. Therm. Fluid Sci.*, 2011, vol. 35, no. 5, p. 825.
3. Iorio, C.S., Goncharova, O.N., and Kabov, O.A., *Microgravity Sci. Technol.*, 2009, vol. 21, no. 1, p. 313.
4. Iorio, C.S., Goncharova, O.N., and Kabov, O.A., *Comput. Therm. Sci.*, 2011, vol. 3, no. 4, p. 333.
5. Lyulin, Yu.V. and Kabov, O.A., *Tech. Phys. Lett.*, 2013, vol. 39, no. 9, p. 795.
6. Lyulin, Yu.V. and Kabov, O.A., *Int. J. Heat Mass Transfer*, 2014, vol. 70, p. 599.
7. Lyulin, Yu.V., Feoktistov, D.V., Afanas'ev, I.A., Chachilo, E.S., Kabov, O.A., and Kuznetsov, G.V., *Tech. Phys. Lett.*, 2015, vol. 41, no. 7, p. 665.
8. Kuznetsov, V.V., *Fluid Dyn. (Engl. Transl.)*, 2011, vol. 46, no. 5, p. 754.
9. Das, K.S. and Ward, C.A., *Phys. Rev. E: Stat., Nonlinear, Soft Matter Phys.*, 2007, vol. 75, 065303.
10. Goncharova, O.N., *Izv. Altai. Gos. Univ.*, 2012, nos. 1–2, p. 12.
11. Margerit, J., Colinet, P., Lebon, G., Iorio, C.S., and Legros, J.C., *Phys. Rev. E: Stat., Nonlinear, Soft Matter Phys.*, 2003, vol. 68, 041601.
12. Andreev, V.K. and Bekezhanova, V.B., *Ustoichivost' neizotermicheskikh zhidkostei* (Stability of Nonisothermal Liquids), Krasnoyarsk: Sib. Fed. Univ., 2010.
13. Goncharova, O.N., Pukhnachov, V.V., and Kabov, O.A., *Int. J. Heat Mass Transfer*, 2012, vol. 54, no. 5, p. 715.
14. Goncharova, O. and Kabov, O., *Dokl. Phys.*, 2009, vol. 54, no. 5, p. 242.
15. Goncharova, O.N. and Kabov, O.A., *Int. J. Heat Mass Transfer*, 2010, vol. 53, p. 2795.
16. Lyubimova, T.P., Lyubimov, D.V., Morozov, V.A., Scurdin, R.V., Ben Hadid, H., and Henry, D., *J. Fluid Mech.*, 2009, vol. 635, p. 275.
17. Nepomnyashchy, A.A. and Simanovskii, I.B., *Phys. Fluids*, 2006, vol. 18, 032105.
18. Goncharova, O.N., Hennenberg, M., Rezanova, E.V., and Kabov, O.A., *Interfacial Phenom. Heat Transfer*, 2013, vol. 1, no. 4, p. 317.
19. Shliomis, M.I. and Yakushin, V.I., *Uch. Zap. Permsk. Gos. Univ., Ser. Gidrodin.*, 1972, no. 4, p. 129.
20. Gebhart, B., Jaluria, Y., Mahajan, R.L., and Sammakia, B., *Buoyancy Induced Flows and Transport*, New York: Hemisphere, 1988, vol. 1.
21. Goncharova, O.N. and Rezanova, E.V., *J. Appl. Mech. Tech. Phys.*, 2014, vol. 55, no. 2, p. 247.
22. Birikh, R.V., *J. Appl. Mech. Tech. Phys.*, 1966, vol. 7, no. 3, p. 43.
23. Andreev, V.K., Gaponenko, Yu.A., Goncharova, O.N., and Pukhnachev, V.V., *Sovremennye matematicheskie modeli konvektsii* (Modern Mathematical Models of Convection), Moscow: Nauka, 2008. 368 c.
24. Joseph, D.D., Stability of fluid motions, vols. 1 and 2, in *Springer Tracts in Natural Philosophy*, Berlin: Springer, 1976, vols. 27 and 28.
25. de Groot, S.R., *Thermodynamics of Irreversible Processes*, New York: Interscience, 1951'
26. Matsiev, L.F. and Stasenko, A.L., *Izv. Akad. Nauk SSSR, Energ. Transp.*, 1987, no. 1, p. 112.
27. Matsiev, L.F., Ryabinina, T.N., and Stasenko, A.L., *Model. Mekh.*, 1987, vol. 1, no. 6, p. 106.
28. Andreev, V.K. and Sobachkina, N.L., *Dvizhenie binarnoi smesi v ploskikh i tsilindricheskikh oblastyakh* (Motion of a Binary Mixture in Planar and Cylindrical Regions), Krasnoyarsk: Sib. Fed. Univ., 2012.
29. Ryzhkov, I.I., *Termodiffuziya v smesyakh: uravneniya, simmetrii, resheniya i ikh ustoichivost'* (Thermodiffusion in Mixtures: Equations, Symmetry, Solutions, and Their Stability), Novosibirsk: Sib. Otd. Ross. Akad. Nauk, 2013.
30. Pukhnachev, V.V., *Izv. Altai. Gos. Univ.*, 2011, nos. 1–2, p. 62.
31. Katkov, V.L., *Prikl. Mat. Mekh.*, 1968, vol. 32, no. 3, p. 482.
32. Goncharova, O.N., *Din. Sploshnoi Sredy*, 1987, no. 79, p. 22.
33. Pukhnachev, V.V., in *Tr. Mezhdun. konf. "Simmetriya i differentsial'nye uravneniya"* (Proc. Int. Conf. on Symmetry and Differential Equations), Krasnoyarsk: Inst. Vychisl. Model., Sib. Otd. Ross. Akad. Nauk, 2000, p. 180.
34. Ostroumov, G.A., *Svobodnaya konvektsiya v usloviyakh vnutrennei zadachi* (Free Convection under Internal Conditions), Moscow: Gos. Izd. Tekh.-Teor. Lit., 1952.
35. Prigozhin, I., *Khimicheskaya termodinamika* (Chemical Thermodynamics), Novosibirsk: Nauka, 1966.
36. Ghezzehei, T.A., Trautz, R.C., Finsterle, S., et al., *Vadose Zone J.*, 2004, no. 3, p. 806.
37. Gatapova, E.Ya. and Kabov, O., *Int. J. Heat Mass Transfer*, 2008, vol. 51, p. 4797.
38. Nakoryakov, V.E., Bufetov, N.S., Grigor'eva, N.I., and Dekhtyar', R.A., *J. Appl. Mech. Tech. Phys.*, 2003, vol. 44, no. 2, p. 236.
39. Pacros, A. and Minster, O., *Microgravity Sci. Technol.*, 2007, vol. 19, nos. 3–4, p. 9.
40. Toth, B., *Microgravity Sci. Technol.*, 2012, vol. 24, p. 189.
41. 3M, 3M™ Novec™ 7100 Engineered Fluid – Data Sheet. http://multimedia.3m.com/mws/mediawebserver?mwsId=SSSSSufSevTsZxtU4Y_G5x_eevUqevTSevTSevTSeSSSSSS–&fn=prodinfo_nvc7100.pdf. Accessed October 1, 2012.
42. Machrafi, H., Sadoum, N., Rednikov, A., Dehaeck, S., Dauby, P.C., and Colinet, P., *Microgravity Sci. Technol.*, 2013, vol. 25, no. 4, p. 251.
43. *Kratkii spravochnik fiziko-khimicheskikh velichin* (Brief Reference Book of Physical and Chemical Quantities), Ravdelya, A.A. and Ponomareva, A.M., Eds., St. Petersburg: Spets. Lit., 1998.

Translated by E. Chernokozhin